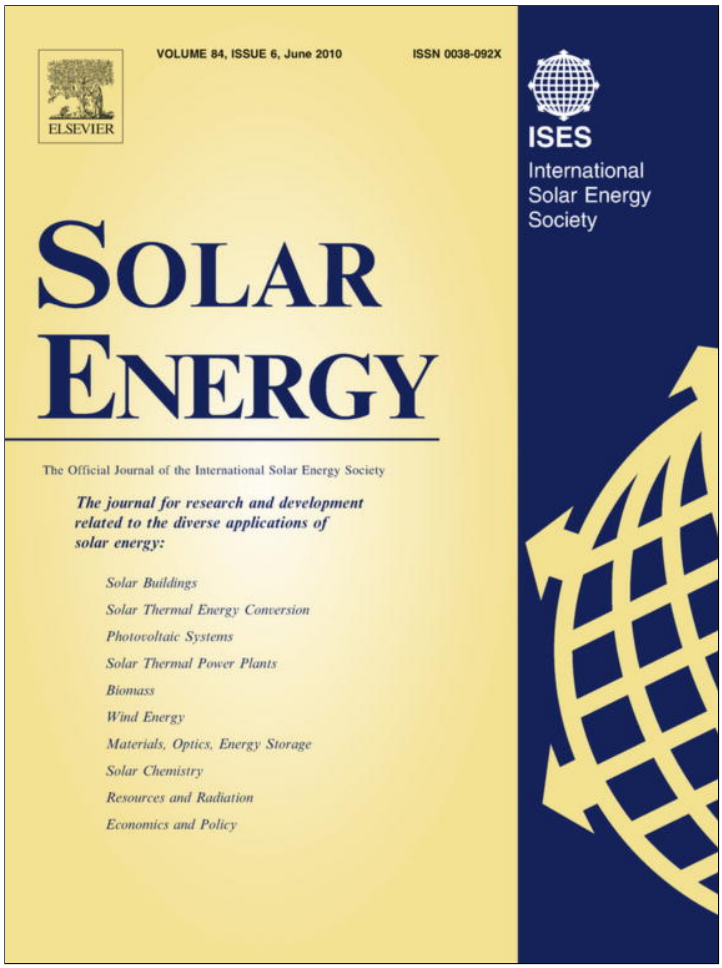

Available online at www.sciencedirect.com
ScienceDirect
Solar Energy 84 (2010) 879–887
SOLAR ENERGY
www.elsevier.com/locate/solener

Foaming of aluminium–silicon alloy using concentrated solar energy

L.E.G. Cambronero [a,*], I. Cañadas [b], D. Martínez [b], J.M. Ruiz-Román [a]

[a] Grupo de Materiales Híbridos, ETSIM-UPM, Madrid, Rios Rosas 21, 28003 Madrid, Spain
[b] Plataforma Solar de Almeria, CIEMAT, P.O. Box 22, 04200 Tabernas (Almeria), Spain

Received 8 August 2008; received in revised form 20 November 2009; accepted 26 November 2009
Available online 25 March 2010

Communicated by: Associate Editor Robert Pitz-Paal

Abstract

Solar energy is used for the work reported here as a nonconventional heating system to produce aluminium foam from Al—Si alloy precursors produced by powder metallurgy. A commercial precursor in cylindrical bars enclosed in a stainless-steel mould was heated under concentrated solar radiation in a solar furnace with varied heating conditions (heating rate, time, and temperature). Concentrated solar energy close to 300 W/cm^2 on the mould is high enough to achieve complete foaming after heating for only 200 s. Under these conditions, the density and pore distribution in the foam change depending on the solar heating parameters and mould design.

Keywords: Aluminium foam; Solar heating; Foaming treatment

1. Introduction

In the last years concentrated solar energy has been applied to materials involved in the following processes: ceramic nanomaterial preparation, synthesis of fullerenes and carbon nanotubes (Flamant et al., 1999), preparation of ceramics with nanograined microstructures (Si_3N_4, SiAlON), simulation of sintering under a wide range of heating rates and isothermal holding times (Zhilinska et al., 2003), fast heating of materials such as SiC/C or C–C, close to thermal shock (Martínez and Rodríguez, 1998a,b), welding, and surface treatments, including TiN coatings to improve titanium wear resistance (García et al., 1998), surface hardening of steel (Flamant et al., 1999), synthesis of YSZ films for fuel cells, hydride formation on zirconium alloys, surface modification on wrought tool steels (Cañadas et al., 2004), sintering of copper (Cañadas et al., 2005) and alumina (Román et al., 2008), etc. Concentrated solar energy can be applied to certain materials using an array of different instruments, for example, a Fresnel lens (García et al., 1998) or a solar furnace such as the one at the PSA-CIEMAT in Almeria (Spain) (Rodríguez et al., 2006) shown in Fig. 1. The advantages of using solar energy (Flamant et al., 1999) include, but are not limited by the following: larger surfaces can be treated than with other photonic systems, high heating rates, low environmental impact and suitability for materials that absorb radiation in the visible spectrum. One disadvantage of using solar energy, on the other hand, is that the energy source intensity can vary over time.

As an alternative to surface material treatment, solar furnaces appear to be a more suitable tool for mass heat treatment when manufacturing aluminium foams. These foams are characterized by their low density due to the distribution of closed cells. They are used as energy, or noise-absorbing materials, and thermal or fire barriers because of their closed pore structure. The two main ways of producing Al foams are gas introduction into the fused alloy (Banhart, 2001) or alternatively, foaming of compacted powders (Banhart, 2005). The most common (and most commercial) route to Al-foaming is directly by gas injection into the melt. The second route consists of heating a precursor

* Corresponding author. Tel.: +34 1 3366995; fax: +34 1 3364177.
E-mail address: luis.gcambronero@upm.es (L.E.G. Cambronero).

0038-092X/$ - see front matter © 2009 Elsevier Ltd. All rights reserved.
doi:10.1016/j.solener.2009.11.014

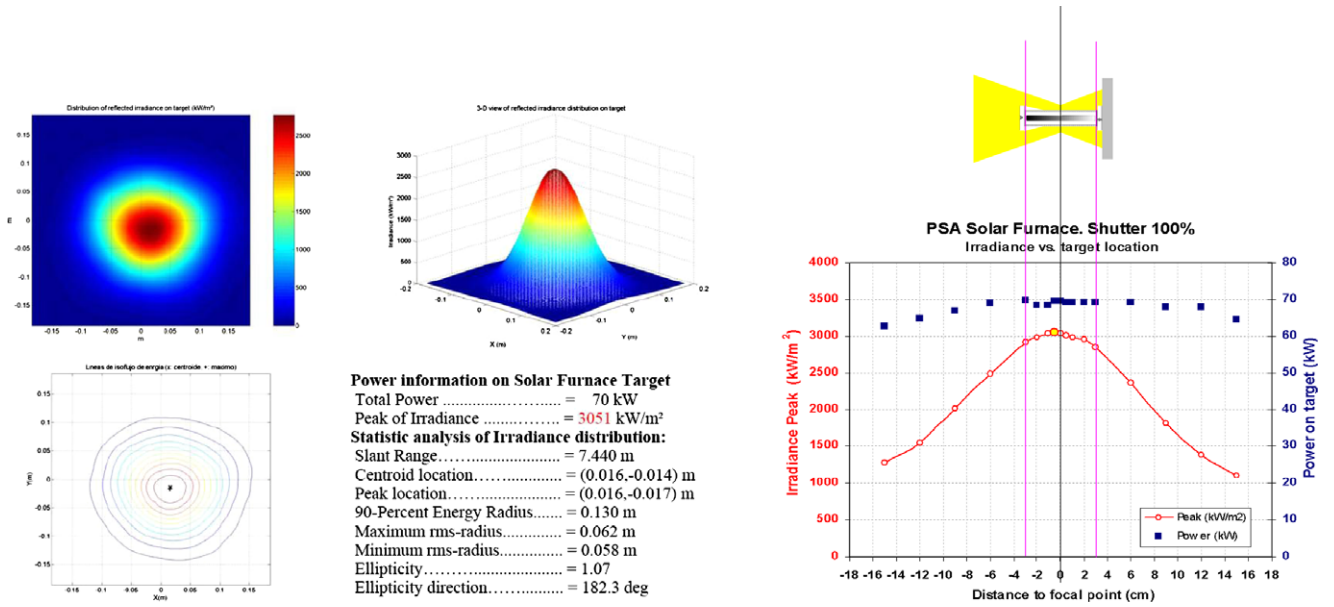

Fig. 1. Left: Power information and flux density in the focus of PSA solar furnace. Right: Solar flux distribution over the sample on horizontal position.

made of scattered foaming agent particles (usually TiH_2) in an aluminium matrix to the melting point. A dense precursor is produced by mixing aluminium powder and titanium hydride, and compacting this mixture, e.g., by hot pressing, extrusion or powder rolling. Then, the temperature of the precursor is raised sufficiently for gas to be released and partly or completely melting the metal. It bubbles and the foam forms. The treatment is then completed by cooling the foam in order to stabilize it. Titanium hydride is widely used in aluminium foam manufacturing since it begins to decompose at about 465 °C, which is below the melting point of aluminium (660 °C) and its alloys, according to the following chemical reaction:

$$TiH_2(s) \rightarrow Ti(s) + H_2(g).$$

When the precursor is cut and placed in a sealed split mould and heated to a temperature slightly above the alloy solidus temperature, high internal pressure voids created by the hydrogen lead to expansion by semi-solid flow, and the aluminium swells, filling the mould with foam. Extruded aluminium crash absorbers with aluminium foam filling is one application of these aluminium foams (Banhart, 2005).

The parameters of closed-mould foaming treatment are heating rate, heating time, preheating temperature and gas environment. Foaming is usually done in ambient air. The heating rate of the un-melted aluminium is limited by furnace capacity and mould and precursor characteristics like conductivity and shape. Furthermore, the heating rate must be as fast as possible to keep the foaming agent from decomposing into gas on the un-melted aluminium, otherwise, cracks appear on the foam cell walls. Different furnace temperatures can also lead to different heating rates and influence the foaming process (Duarte and Banhart, 2000; García Cambronero et al., 2008). Thus, higher heating rates lead to earlier expansion of the foamable precursor, due to the fact that the melting temperature is reached sooner. On the other hand, slower heating decreases foamability due to gas lost during titanium hydride decomposition and oxidation, which could produce non-metal layers on the surface (Duarte and Banhart, 2000).

One major innovative feature of this work consists of replacing the conventional preheated electric furnace with concentrated solar energy, which is used to heat the whole precursor and mould. Solar heating is more economical for powder metallurgy processing of aluminium foams than conventional heating on electric heating plates, and would therefore, lower the cost of powder metallurgy manufacturing thereby making it more competitive than the melt route for aluminium foams manufacturing.

2. Experimental procedure

2.1. Solar furnace conditions

Experiments were carried out in a solar furnace located at the PSA-CIEMAT in Almeria, Spain. A solar furnace is a high-concentrating facility consisting essentially of a flat heliostat, a parabolic concentrator mirror, a shutter and the test bed located in the concentrator focus. A flat collecting mirror, or heliostat, tracks the sun and reflects the parallel horizontal solar beams onto the parabolic concentrator, which in turn reflects the solar beams onto the focus (the test bed). The heliostat is computer controlled and tracks the sun continuously. It is designed to work properly at wind speeds up to 50 km/h with occasional strong gusts. The incoming parallel rays from the heliostat are concentrated by the parabolic dish, multiplying the radiation flux in the focus. The parabolic dish consists of 98 spherical facets which dimensions are 1.222 m × 0.917 m, distributed by their curvature radii in

Fig. 2. General furnace view (left) and test table with re-directional mirror (right) during foaming testing at PSA.

five concentric circles around the centre of the parabola. The total reflecting area is 98 m^2, reflectivity 92%, peak flux 3000 kW/m^2, focus diameter 26 cm, and focus length 7.45 m (Rodríguez et al., 2006).

The shutter, located between the concentrator and the heliostat, regulates the amount of light aimed at the dish and thereby, the solar power at the focus. A test table in the focus is movable in three directions, east–west, north–south, up and down (Z-direction), placing the test samples in the focus with great precision (Martínez and Rodríguez, 1998a,b). A solar furnace is characterized by the parabolic dish and its flux density distribution in the focus, which usually has a Gaussian geometry, as characterized by a CCD camera hooked up to an image processor and a lambertian target (Fig. 1, Monterreal, 2005).

Closed mould tests were carried out in an air atmosphere without any sample-holder (hot plate) displacement and under direct normal irradiance (DNI) close to 1000 W/m^2. Under clear sky conditions, solar irradiation received in Almeria is up to 1040 W/m^2. With a standard DNI of 1000 W/m^2, the peak flux density is close to 300 W/cm^2 with 100% shutter aperture (Monterreal, 2005). Direct solar heating solar testing without closed metallic mould, had the following configuration with the sample placed in a horizontal position and the incident concentrated radiation redirected at a 90° angle over the test table by a tilted mirror, as shown in Fig. 2.

Fig. 3 shows how a 5 mm diameter Al + 1%TiH_2 precursor made by powder metallurgy (Cambronero et al., 2004) was placed on an alumina plate with two thermocouples. A graphite coating on the precursor improved heat transfer.

During testing, the test table was placed in the focus, at different Z positions, for each test in order to find out the best position for controlling the heating cycle. Once the sample is placed in the right focal position, the test is started. Solar furnace test variables were maximum shutter aperture of 25%, being the facility maximum peak flux density close to 300 W/cm^2, test table movement in Z-direction from 0 to 75 mm, heating time from 90 to 300 s, heating temperature between 700 and 730 °C and air cooling. Power close to 300 W was applied to the cylindrical mould surface through the top plate under these shutter aperture and flux density conditions. The precursor was inserted vertically in a 20-mm-inner-diameter stainless-steel mould (as seen in Fig. 4). The mould was then placed on the test table in a position such that the focus is directly over the mould, and a mirror redirected the concentrated solar radiation onto the top of the test piece, since the PSA solar furnace has a horizontal axis. The secondary mirror is then water-cooled to avoid thermal shock and overheating.

2.2. Stainless-steel mould specifications

The purpose of the mould is not only to absorb the concentrated solar energy as it happens with other devices such as open volumetric solar receivers (Fend et al., 2004) and transfer its heat to the AlSi12 precursor, but also to control the shape of the foam. When direct concentrated sunlight was applied directly to a 5 mm-diameter Al + 1%TiH_2 pre-

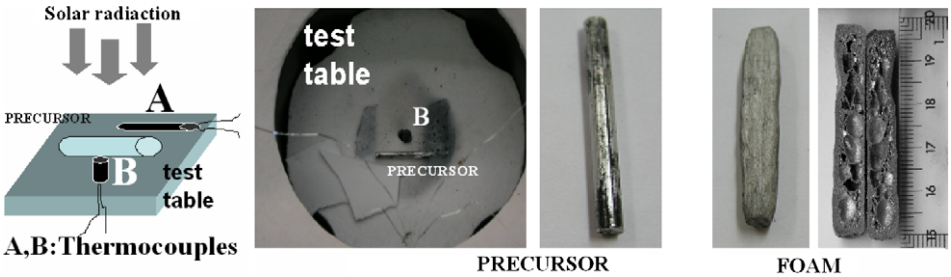

Fig. 3. Al + 1%TiH_2 precursor of 5-mm-diameter and foam obtained by direct solar heating.

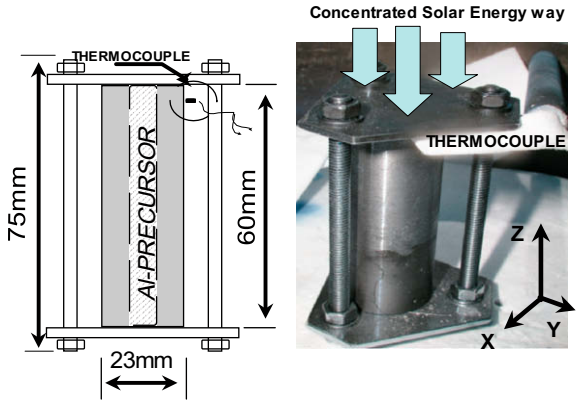

Fig. 4. Drawing of the closed metal mold with 60-mm long precursor (left) and photograph of the arrangement of the closed metal mold on the hot plate (right).

cursor, control of the final foam dimension and shape was poor and required the temperature to be measured by indirect techniques, as shown in Fig. 4, making it more difficult to control heating.

A closed mould placed on an alumina support was therefore used to make cylindrical foams as shown in Fig. 4. The steel support surface and the thermocouple are protected by alumina, so only the sample and the mould are treated with concentrated solar energy (Cañadas et al., 2004). The stainless-steel mould is made of 316 stainless-steel with a 150 g mass. This material shows a good absorbance to solar radiation. It has a 4.15 cm^2 cylindrical section and a 20 mm-diameter hole. This design is based on the one used by Helwig and Banhart (2003).

2.3. Test performance and temperature control

The temperature profile on the precursor was measured by thermocouples placed 5 mm from the top and 5 mm from the bottom of a 6 cm-long precursor. During foaming tests, the reference temperature was measured by a thermocouple placed in a hole at the top of the stainless-steel cylinder and protected from the solar beam by insulation. The 21.60 cm^2 upper plate is painted with graphite to improve heating efficiency by increasing its absorptivity.

The heating rate can be modified by varying the shutter aperture and focus position Z, which modifies flux density. After several tests, the optimal focus position was found to be $Z = 60$ mm. With the on-target power, shown in Fig. 1, a focus position Z close to 60 mm on the test table located the focus in the centre of the mould. However, the mould design causes it to be heated at a higher rate on top due to the upper mould surface, meaning that there is clearly a temperature gradient during the test.

Although a wider shutter aperture leads to a faster heating rate, a uniform increase in temperature can only be attained via step-by-step increases in shutter aperture (see Fig. 6). Using this procedure, temperatures of up to 700–735 °C were reached in 90–120 s. The fastest heating rate in this test was found with a shutter aperture of about 20%, but temperature inertia is controlled more adequately with small shutter apertures. Supplementary tests carried out on 6-cm-long precursor bars in an electric furnace preheated to 750 °C characterized the behaviour and measured the thermal gradient on the precursor.

2.4. Aluminium foam manufacturing and characterization

The precursor for this test was a commercial Al–12%Si 1%TiH_2 made by powder metallurgy. The melting point of this alloy is close to 580 °C and the eutectic point of the Al–Si alloy is 577 °C. Before solar heating, precursors were coated with graphite to make demoulding easier after foaming. The cylindrical precursor bars used were 60 mm long with a 10 mm diameter.

The foam structure was analysed as a function of both precursor length and the heating cycle applied to the mould. It was shown that relative density is the most important variable and a power law function can successfully describe the dependence of electrical conductivity of aluminium alloy foams on the relative density (Feng et al., 2002). Other properties, such as moduli, strength, and electrical conductivity of closed-cell foams are close to predictions for open-cell foams, mainly because the cell face has very little influence on these properties. Relative foam conductivity σ/σ_s depends on relative density ρ/ρ_s: $\sigma/\sigma_s = \alpha[\rho/\rho_s] + (1-\alpha)[\rho/\rho_s]^{3/2}$, where σ is the foam conductivity, σ_s is the solid conductivity, ρ is de foam density, and ρ_s is the solid density. $\alpha = 0.05$ fits the data for closed-cell foams well (Ashby et al., 2000). This correlation between foam density and electrical conductivity allows the foam structure to be analysed using an eddy current device, as the parts with less foam degree have higher conductivity.

Foam densities and dimensional change in volume due to foaming were determined by the Archimedes method. An increase in volume of close to 280% would be needed for the precursor to fill the entire mould. Foams were precisely cut along their generatrices to study their cell structure and the influence of the solar furnace parameters on foam development. Eddy-current conductivity was measured in cross sections with an 8 mm test probe at 60 MHz at room temperature.

3. Results and discussion

3.1. Temperature distribution during foaming

Results of an exploration test using a preheated electrical furnace are shown in Fig. 5. Mould heating follows a parabolic curve over time. Therefore, a constant heating rate cannot be achieved. The heating rate is higher on the bottom of the mould due to thermal conductivity through the hot plate. The average thermal gradient between the top and bottom of the mould is less than 40 °C during heating, however, no temperature gradient was observed in precursors up to their melting point, close to 580 °C, with a

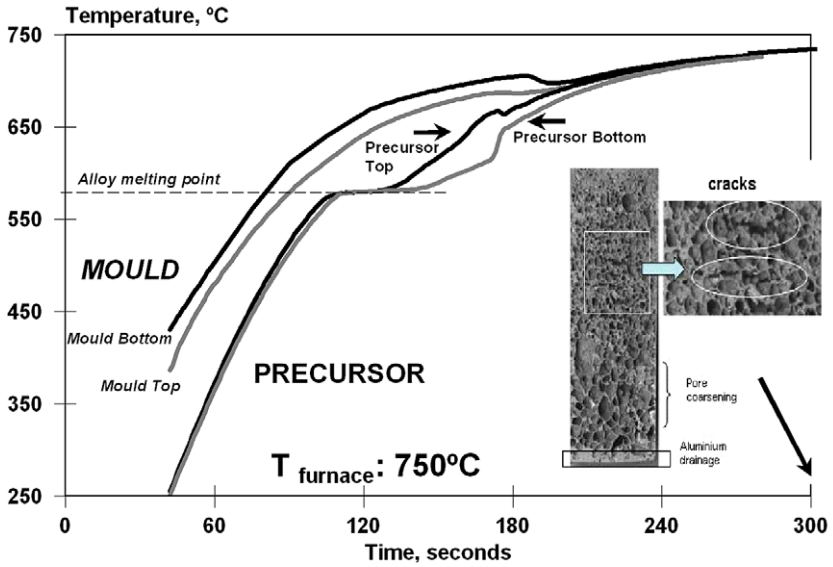

Fig. 5. Thermal gradient on mould and precursor during foaming treatment on preheated electrical furnace and foam structure obtained at foaming time of 300 s.

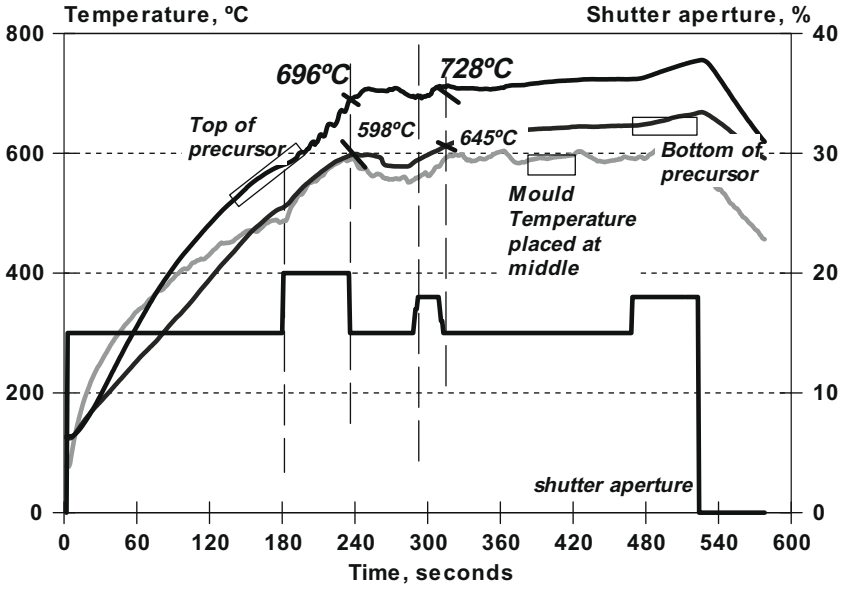

Fig. 6. Temperature gradient on precursor during solar heating in solar furnace.

heating rate close to 4.5 °C/s up to this temperature. Precursor melting, on one hand, smoothes out at its melting point (580 °C), as reported by Helwig and Banhart (2003), and on the other, temperature on the mould decreases as soon as the test time is close to 180 s – when foam expansion comes into contact with the mould wall. After a heating time of 200 s, there was no temperature gradient between the two thermocouples at the top and bottom of the original precursor. If foam treatment is interrupted after 300 s by removing the mould from the furnace and cooling it with air, the resulting foam structure is as shown in Fig. 5. Thus it can be seen through this exploration test that faster heating times lead to foam collapse.

The temperature gradients in the solar furnace on the same mould, with the same precursor length and thermocouple positions, are shown in Fig. 6. The heating rate was controlled by the precursor temperature to achieve constant heating. Mould temperature did not increase at a constant rate, but followed a parabolic curve. Since heat is applied to the top of the mould, a temperature gradient forms along the precursor during the test. When the melting point (580 °C) was reached, differences in the temperature in the precursor were close to 98 °C, and 83 °C at the end of the test. Thus, the precursor heats up on top at 2.1 °C/s and on the bottom at 2.52 °C/s. After the precursor melted on top, the heating rate decreased to 1.8 °C/s, at

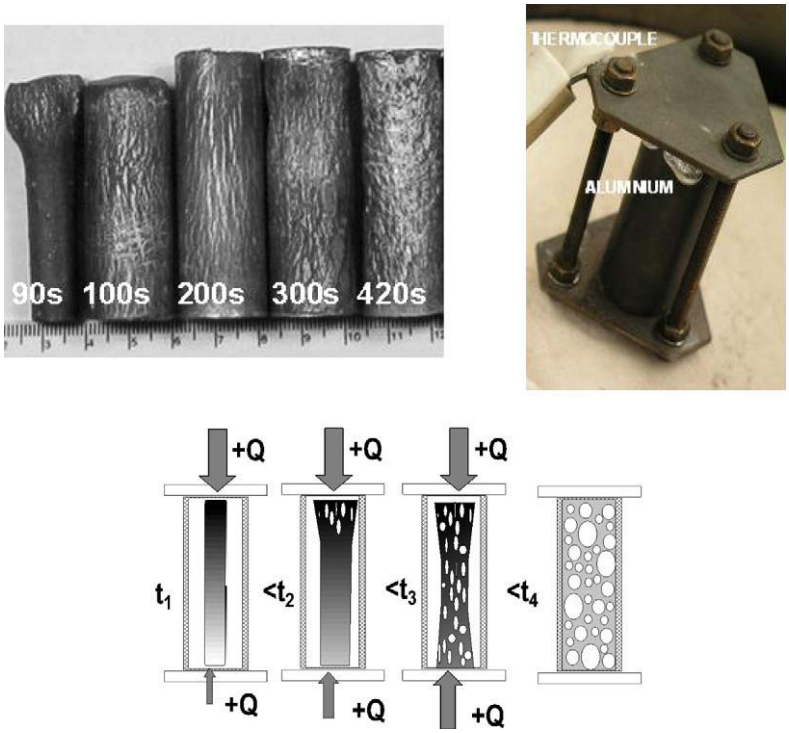

Fig. 7. Foam evolution on 60 mm long precursor a function of foaming time (left) and a drawing of foam evolution with the heating (right).

which point the shutter aperture was opened to 20% to keep the heating rate up and reach 700 °C. Therefore, due to this increase in power, no interval of constant temperature from aluminium melting was recorded the way it was in the electrically preheated furnace (see Fig. 5). Certainly latent heat effects occur in case of preheated reference furnace, but these effects can be compensated by increasing irradiation in case of a shutter-controlled solar furnace. Also AlSi12 melting is to use an open mould and a CCD camera on solar furnace (Cambronero et al., 2006). After the precursor foams, the temperature gradient in the precursor rises up to the end of the test, especially when the shutter is closed and air starts cooling. Under these heating conditions, foam collapsed, and aluminium drained and spilled.

3.2. Foam structure development

Foaming tests were conducted at heating rates close to 5.5 °C/s up to around 700 °C, in which temperatures were measured on top of the mould. This heating rate is higher than in the precursor temperature gradient test, and so the temperature gradient can be expected to be higher than in Fig. 6. Once the foaming temperature is reached, a shutter aperture of $20 \pm 5\%$ keeps the power constant during the test. After closing the shutter, the mould was air-cooled before removing from the solar furnace test table, which decreased the risk of collapse due to the mould shaking while the foam was still liquid. These effects can be also avoided by conventional techniques, such as by lifting a tube furnace, or using induction or infrared heating.

During heating, heat flows from the mould into the precursor at both ends where mould and precursor are in contact. Fig. 7 is a graphical drawing which shows the foaming with respect to time. The heating cycles of these samples are presented in Figs. 8 and 9. Due to the solar beam path, the precursor starts heating faster at the top rather than at the bottom. At this point, elongated pores are formed at the beginning of foaming due to the precursor extrusion path. As foaming expansion improves, rounded pores are also formed. Again, time and temperature control the foaming process. In Fig. 8, Curve A, cell foam structure can be seen to start at the top of the precursor. Foam expansion is improved when temperature is increased along Curve B, Fig. 8. When heating time is increased, as in Fig. 9 Curves B and C, the foam structure forms on the bottom of the precursor first and, to a lesser degree, in the middle, due to nonuniform distribution of heat along the precursor. Sections of foam structure formation over time can be seen in Fig. 10.

If the foam structure is not fully developed at the set preheated furnace temperature, heating time has to be increased. The only problem with temperature increase is the possibility of overheating, which makes the structure unstable, coarsening its cells, spilling aluminium, and releasing gas, collapsing the foam structure. Some of these defects can be seen in Fig. 5, when precursor heating time was too high. Precursor composition also modifies the foaming parameters. Low-melting-point aluminium alloys keep gas from being released in the un-melted aluminium, as does faster heating. Addition of calcium or calcium compounds to the aluminium increases melt viscosity and

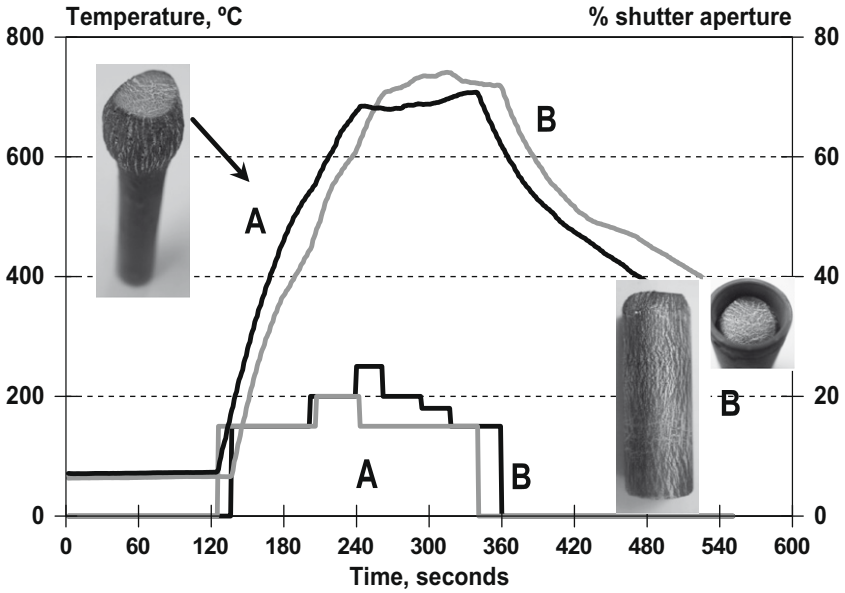

Fig. 8. Heating cycle at different foaming times to achieve the a non completed foams after 90 s (Curve A) and 100 s (Curve B).

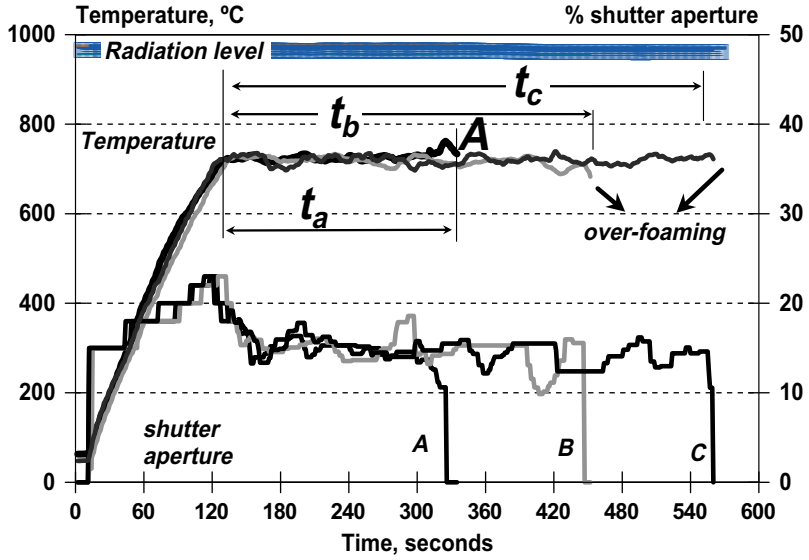

Fig. 9. Heating cycle of foams showed on Fig. 7 at different foaming times: 200 s (ta) 300 s (tb) and 420 s (tc).

makes the foam structure more stable during the liquid state (Arnold et al., 2003; Cambronero et al., 2006).

Pore distribution and electrical conductivity in the foam are different with different heating times as observed in Fig. 10. Electrical conductivity through the foam depends on pore distribution and size, and aluminium areas due to aluminium drainage. This is caused by the flow of liquid metal through the foam driven by capillary forces and gravity during foaming. In Fig. 10, when foam was formed after 200 s of heat treatment, high electrical conductivity was found in aluminium drainage areas, whereas low electrical conductivities were found in areas of very coarse pores, confirming the relationship between density and electrical conductivity in aluminium foam (Ashby et al., 2000). A property gradient was also found after 100 s (Fig. 10), when density and conductivity are higher in the middle of the sample, where there is less degree of foaming agent decomposition. Mould design and heating conditions thus cause a functional gradient in analysed material properties.

Fig. 10 shows that after an optimal heating time of almost 200 s, cell structure density is close to 0.7 g/cm^3 (Table 1) and foam expands 285%, filling the mould. The foam structure showed some cell wall fissures that might appear in a preheated furnace. These foam defects are also present in AlSi foams formed in a preheated electric fur-

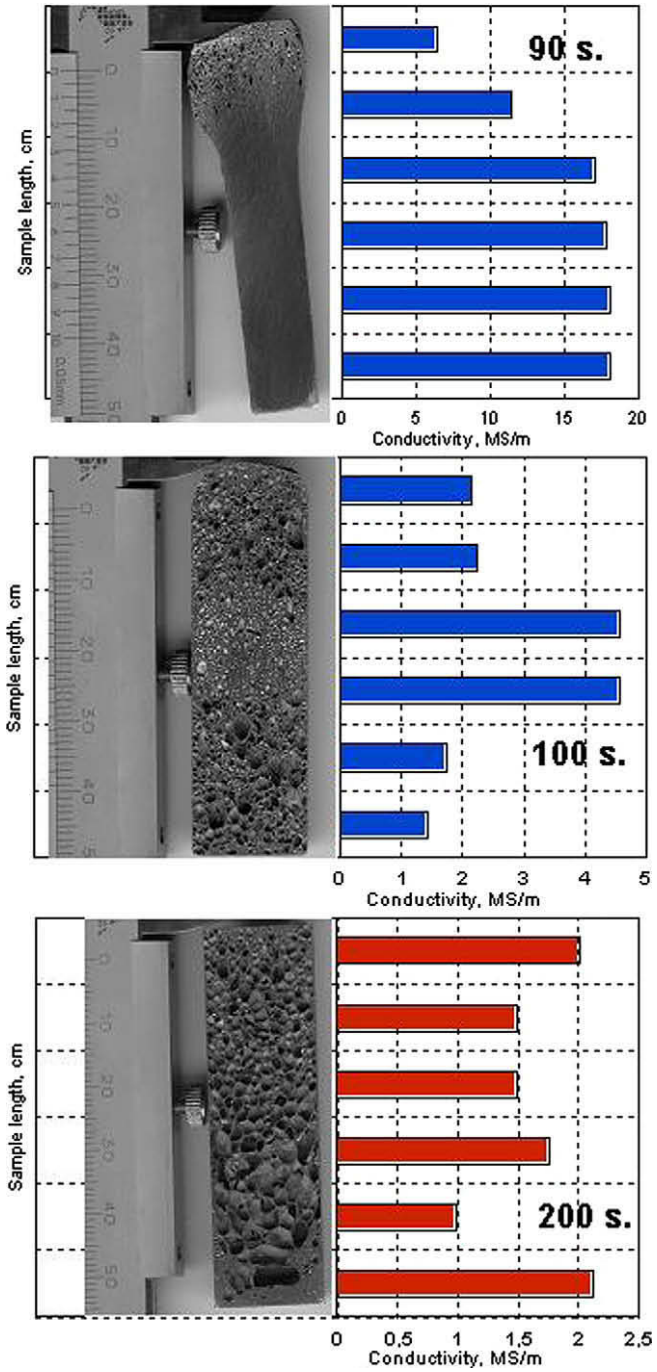

Fig. 10. Conductivity across the foam section showed on Fig. 7 after three different heating times (90, 100, and 200 s) at 700–725 °C.

Table 1
Changes in density and dimensions of aluminium precursors after foaming.

Temperature (average) °C	700	725	725	725	725
Foaming time, s	90	100	200	300	420
Density, g/cm^3	1,74	0,77	0.71	0,61	0,74
Volume change%	16	257	284	253[a]	180[a]

[a] During foaming aluminium is spilling from the mold and foam showed a collapsed structure.

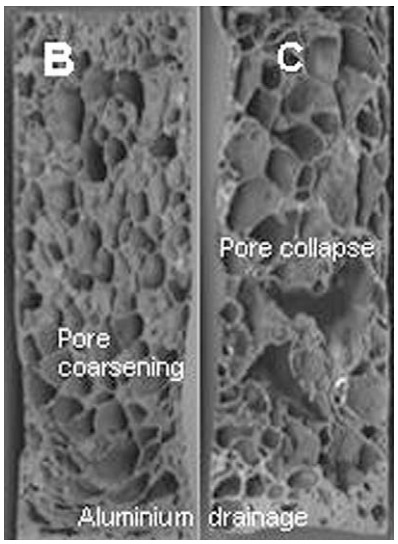

Fig. 11. Foam structure of over foaming precursors at foaming times of 300 s (tb), sample B, and 420 s (tc) sample C.

nace as observed in Fig. 5 after a 300 s heat treatment. Total foaming time is also close to the one used in a pre-heated furnace, which requires around 100 s to achieve the foaming temperature. A faster heating rate should be used to decrease the heat treatment time and also to reduce cracking due to foaming agent decomposition in a non-melting aluminium matrix. Also faster cooling is available on solar furnace hot plate and a lower metal flow should be expected as well as a decrease on aluminium drainage.

As seen in Fig. 11, in addition to cell cracking, other defects, such as pore collapse due to excessive foaming time appear as foam density increases and volume expansion decreases (Table 1), as well as aluminium spilling and drainage. Aluminium foams collapse (Duarte and Banhart, 2000) is caused by two mechanisms, drainage, or leakage of molten metal from the cell walls by gravity, and cell coalescence, when two cells merge to form one large one, probably due to cell rupture.

4. Conclusions

Concentrated solar energy is a suitable way to foam AlSi12 precursors at a constant heating rate by controlling the shutter aperture of the Solar Furnace and latent heat effects can be compensated by increasing irradiation power. This constant heating rate cannot be achieved in a pre-heated electric furnace. However, the precursor did not reach its melting point at the same time with the increased power provided by opening the shutter aperture further as it did in the preheated furnace heating cycle. Since temperature was controlled in a closed metal mould, a thermal gradient appeared in the precursor during the test. Foam structure is a function of how this metal mould is heated and how heat is transferred to the AlSi12 precursor. The air cooling rate also maintains the newly-formed foam structure.

Once the mould design and the stainless-steel to be used for it, and the table position for adequate flux density have been decided, a continuously controlled shutter aperture provides continuous heating of the mould. The time frame for foaming of 60 mm-long precursors is completed in 200 s. Foaming starts at the top of the precursor and proceeds from both ends of the sample due to the mould design. This allows a gradient in material properties to be achieved and thus, functionally graded foams can be formed. As expected, similar to conventional processing, excessive heat treatment time leads to foam defects, such as aluminium spillage and drainage and cell coarsening, which are also found in conventional preheated electric furnaces. Pores will not collapse in foams formed by concentrated solar heat treatment as they do when the mould is removed from electric furnaces.

Acknowledgements

This research was carried out under Spanish CICYT Project MAT 2003-08873-C03-02 and National R&D Programme Projects MAT 2006-13347-C03-02 and REN 2003-09247-C04-01/TECNO.

References

Arnold, M., Kroner, C., Singer, R.F., 2003. PM aluminium foams: stabilizing mechanisms and optimisation. Proceedings Metfoam03, Berlin, 23–25 June, 371–376.

Ashby, M.F., Evans, A.G., Fleck, N.A., Gibson, L.I., Hutchinson, J.W., Wadley, H.N.G., 2000. Metal Foams. A design guide. Elsevier, Butterworth-Heineman, p. 193.

Banhart, J., 2001. Manufacture, characterisation and application of cellular metals and metal foams. Prog. Mater. Sci. 46, 559–632.

Banhart, J., 2005. Aluminium foams for lighter vehicles. Int. J. Vehicle Des. 37 (2/3), 114–125.

Cambronero, L.E.G., Ruiz-Roman, J.M., Ruiz-Prieto, J.M, Sanchez, M., Ranninger, C., 2004. Obtención de espumas de Al–7Si–1Mg a partir de polvos obtenidos mediante aleación mecánica. Proc. VIII Con. Nac. Mat. Valencia, Spain, June 15–17, 224–226.

Cambronero, L.E.G., Diaz, J.J., Ruiz-Roman, J.M., Corpas, F.A., Ruiz-Prieto, J.M., 2006. Influencia de la adición de compuestos de calcio sobre el desarrollo de la estructura celular de espumas de aluminio y AlSi12. Proceedings IX Con. Nac. Mat. 19–22 Julio, Vigo, Spain, 559–562.

García Cambronero, L.E., Cañadas, I., Diaz, J.J., Ruiz Román, J.M., Martinez, D., 2008. Tratamiento térmico de espumación de precursores de aluminio-silicio en horno solar de lecho fluidificado. Proceedings X Con. Nac de Materiales 16–16 Junio2008. 261–264.

Cañadas, I., Martínez, D., Rodríguez, J., 2004. Tratamiento térmico de materiales en el Horno solar de la PSA: líneas actuales de actividad. Bol. Soc.E. Cer. y V. 43 (2), 591–595.

Cañadas, I., Martínez, D., Rodríguez, J., Gallardo, J.M., 2005. Aplicación de la Radiación Solar Concentrada al Proceso de Sinterizado de Cobre. Rev. Metal. Madrid, 165–169.

Duarte, I., Banhart, J., 2000. A study of aluminium foam formation kinetics and microstructure. Acta Mater. 48, 2349–2362.

Feng, Y., Zheng, H., Zhu, Z., Zu, F., 2002. The microstructure and electrical conductivity of aluminum alloy foams. Mater. Chem. Phys. 78, 196–201.

Fend, T., Hoffschmidt, B., Pitz-Paal, R., Reutter, O., Rietbrock, P., 2004. Porous materials as open volumetric solar receivers: Experimental determination of the thermophysical and heat transfer properties. Energy 29, 822–823.

Flamant, G., Ferriere, A., Laplaze, D., Monty, C., 1999. Solar processing of materials: opportunities and new frontiers. Solar Energy 566 (2), 117–132.

García, I., Sánchez-Olias, J., Damborenea, J.J., Vázquez, A.J., 1998. Síntesis de nitruro de titanio mediante láser y energía solar concentrada. Rev. Metal. Madrid 34 (2), 109–113.

Helwig, H.M., Banhart, J., 2003. Heat distribution during metal foaming. Proceedings Metfoam03, Berlin, 23–25 June, 165–168.

Martínez, D., Rodríguez, J., 1998a. Surface treatment by concentrated solar energy: the solar furnace al the "Plataforma Solar de Almería". Surf. Modif. Technol. XI, 441–447.

Martínez, D., Rodríguez, J., 1998b. Tratamiento superficial de materiales mediante luz solar concentrada: una opción mediante energías renovables. Rev. Metal. Madrid 34 (2), 104–113.

Monterreal, R., 2005. Preliminar analysis of irradiance distribution shutter-100%. PSA Internal Document.

Rodríguez, J., Cañadas, I., Fernández, J., Monterreal, R., Ballestrín, J., Téllez, F., Yebra, L., 2006. The PSA solar furnace, a test facility ready to characterize high-concentration solar devices from solar thermal applications to PV cells. Proceedings of 13th International Symposium on Concentrated Solar Power and Chemical Energy Technologies.

Román, R., Cañadas, I., Rodríguez, J., Hernández, M.T., González, M., 2008. Solar sintering of alumina ceramics: microstructural development. Solar Energy 82, 893–902.

Zhilinska, N., Zalite, I., Rodriguez, J., Martínez, D., Cañadas, I., 2003. Sintering of nanodisperse powders in a solar furnace. Proceedings EURO PM, 423–428.